

 Open access • Posted Content • DOI:10.1101/2020.08.18.255935

## **IFITM proteins promote SARS-CoV-2 infection of human lung cells** — [Source link](#)

[Caterina Prelli Bozzo](#), [Rayhane Nchioua](#), [Meta Volcic](#), [Lukas Wettstein](#) ...+22 more authors

**Institutions:** [University of Ulm](#), [Charité](#), [Kyoto University](#)

**Published on:** 18 Aug 2020 - [bioRxiv](#) (Cold Spring Harbor Laboratory)

**Topics:** [Interferon](#)

Related papers:

- [SARS-CoV-2 Cell Entry Depends on ACE2 and TMPRSS2 and Is Blocked by a Clinically Proven Protease Inhibitor](#)
- [IFITM proteins promote SARS-CoV-2 infection in human lung cells](#)
- [IFITM dependency of SARS-CoV-2 variants of concern](#)
- [Distinct patterns of IFITM-mediated restriction of filoviruses, SARS coronavirus, and influenza A virus.](#)
- [Clinical features of patients infected with 2019 novel coronavirus in Wuhan, China](#)

Share this paper:    

View more about this paper here: <https://typeset.io/papers/ifitm-proteins-promote-sars-cov-2-infection-of-human-lung-4fmkssiixp>

# 1 **IFITM proteins promote SARS-CoV-2 infection**

## 2 **and are targets for virus inhibition**

3 Caterina Prelli Bozzo<sup>1#</sup>, Rayhane Nchioua<sup>1#</sup>, Meta Volcic<sup>1</sup>, Jana Krüger<sup>2</sup>, Sandra Heller<sup>2</sup>,  
4 Christina M. Stürzel<sup>1</sup>, Dorota Kmiec<sup>1,3</sup>, Carina Conzelmann<sup>1</sup>, Janis Müller<sup>1</sup>, Fabian Zech<sup>1</sup>,  
5 Desiree Schütz<sup>1</sup>, Lennart Koepke<sup>1</sup>, Elisabeth Braun<sup>1</sup>, Rüdiger Groß<sup>1</sup>, Lukas Wettstein<sup>1</sup>,  
6 Tatjana Weil<sup>1</sup>, Johanna Weiß<sup>1</sup>, Daniel Sauter<sup>1,4</sup>, Jan Münch<sup>1</sup>, Federica Diofano<sup>5</sup>, Christine  
7 Goffinet<sup>6</sup>, Alberto Catanese<sup>7</sup>, Michael Schön<sup>7</sup>, Tobias Böckers<sup>7</sup>, Steffen Stenger<sup>8</sup>, Kei Sato<sup>9</sup>,  
8 Steffen Just<sup>5</sup>, Alexander Kleger<sup>2</sup>, Konstantin M.J. Sparrer<sup>1\*</sup> and Frank Kirchhoff<sup>1\*</sup>

9  
10 <sup>1</sup>Institute of Molecular Virology, Ulm University Medical Centre, 89081 Ulm, Germany.

11 <sup>2</sup>Department of Internal Medicine I, Ulm University Medical Centre, 89081 Ulm, Germany.

12 <sup>3</sup>Department of Infectious Diseases, King's College London, WC2R 2LS London, United  
13 Kingdom. <sup>4</sup>Institute of Medical Virology and Epidemiology of Viral Diseases, University  
14 Hospital Tübingen, 72076 Tübingen, Germany. <sup>5</sup>Department of Internal Medicine II  
15 (Cardiology), Ulm University, 89081 Ulm, Germany. <sup>6</sup>Institute of Virology, Charité -  
16 Universitätsmedizin Berlin, 10117 Berlin, Germany. <sup>7</sup>Institute for Anatomy and Cell Biology,  
17 Ulm University, 89081 Ulm Germany. <sup>8</sup>Institute of Medical Microbiology and Hygiene, Ulm  
18 University Medical Centre, 89081 Ulm, Germany. <sup>9</sup>Institute of Medical Science, The  
19 University of Tokyo, 1088639 Tokyo, Japan.

20  
21 # both contributed equally to this work

22 \* Address Correspondence to:

23 [konstantin.sparrer@uni-ulm.de](mailto:konstantin.sparrer@uni-ulm.de) or [Frank.Kirchhoff@uni-ulm.de](mailto:Frank.Kirchhoff@uni-ulm.de)

24  
25 Running title: IFITMs promote SARS-CoV-2 infection

26  
27 **KEYWORDS:** SARS-CoV-2, Interferon-induced transmembrane proteins, spike  
28 glycoproteins, human lung cells, viral entry cofactors

29 Interferon-induced transmembrane proteins (IFITMs 1, 2 and 3) are thought to restrict  
30 numerous viral pathogens including severe acute respiratory syndrome coronaviruses (SARS-  
31 CoVs). However, most evidence comes from single-round pseudovirus infection studies of  
32 cells that overexpress IFITMs. Here, we verified that artificial overexpression of IFITMs  
33 blocks SARS-CoV-2 infection. Strikingly, however, endogenous IFITM expression was  
34 essential for efficient infection of genuine SARS-CoV-2 in human lung cells. Our results  
35 indicate that the SARS-CoV-2 Spike protein interacts with IFITMs and hijacks them for  
36 efficient viral entry. IFITM proteins were expressed and further induced by interferons in  
37 human lung, gut, heart and brain cells. Intriguingly, IFITM-derived peptides and targeting  
38 antibodies inhibited SARS-CoV-2 entry and replication in human lung cells, cardiomyocytes  
39 and gut organoids. Our results show that IFITM proteins are important cofactors for SARS-  
40 CoV-2 infection of human cell types representing in vivo targets for viral transmission,  
41 dissemination and pathogenesis and suitable targets for therapeutic approaches.

## 42 INTRODUCTION

43 SARS-CoV-2 is the cause of pandemic Coronavirus disease 2019 (COVID-19). Originating  
44 from China in late 2019, the virus has infected more than 76 million people around the globe  
45 (<https://coronavirus.jhu.edu/map.html>). While SARS-CoV-2 spreads more efficiently than  
46 SARS-CoV and MERS-CoV, the previously emerging causative agents of severe acute  
47 respiratory syndromes (SARS), it shows a lower case-fatality rate (~2 to 5%), compared to  
48 ~10% and almost 40%, respectively<sup>1-3</sup>. The reasons for this efficient spread and the  
49 mechanisms underlying the development of severe COVID-19 are incompletely understood  
50 but the ability of SARS-CoV-2 to evade or counteract innate immune mechanisms may play a  
51 key role<sup>4</sup>.

52 Here, we focused on innate immune effectors that are thought to target the first essential step  
53 of SARS-CoV-2 replication: entry into its target cells. A prominent family of interferon (IFN)  
54 stimulated genes (ISGs) known to inhibit fusion between the viral and cellular membranes are  
55 interferon-inducible transmembrane (IFITM) proteins<sup>5,6</sup>. The three best characterised members  
56 of the IFITM family are IFITM1, IFITM2 and IFITM3<sup>7-10</sup>. They contain different sorting  
57 motifs and IFITM1 is mainly localised at the plasma membrane, while IFITM2 and 3 are found  
58 inside the cell on endo-lysosomal membranes<sup>7</sup>. Thus, IFITM proteins may act at different sites  
59 of viral entry and it has been reported that they restrict multiple classes of enveloped viral  
60 pathogens including Influenza A viruses, Flaviviruses, Rhabdoviruses, Bunyaviruses and  
61 human immunodeficiency viruses<sup>6,11</sup>. The molecular mechanism(s) underlying the antiviral  
62 activity of IFITMs are not fully understood. However, recent reports suggest that they modulate  
63 membrane rigidity and curvature to prevent fusion of the viral and cellular membranes<sup>12-14</sup>.

64 It has also been reported that IFITM proteins inhibit human coronaviruses including SARS-  
65 CoV-1 and SARS-CoV-2 as well as MERS-CoV<sup>11,15</sup>. However, most results were obtained  
66 using Spike containing viral pseudoparticles and cell lines overexpressing the IFITM proteins  
67 and frequently also the viral ACE2 receptor. Here, we confirmed and expanded previous results

68 showing that IFITM proteins block SARS-CoV-2 entry under such artificial experimental  
69 conditions. In striking contrast, however, endogenous IFITM proteins were essential for  
70 efficient infection and replication of genuine SARS-CoV-2 in various types of human cells.  
71 We found that IFITM proteins are expressed in human cell types involved in virus transmission,  
72 dissemination to various organs, and development of severe COVID-19. In further support of  
73 an important role of IFITM proteins as entry cofactors of SARS-CoV-2, IFITM-derived  
74 peptides and targeting antibodies efficiently inhibited SARS-CoV-2 infection of human lung,  
75 heart and gut cells. Our unexpected finding that SARS-CoV-2 hijacks human IFITM proteins  
76 for efficient infection helps to explain the rapid spread of this pandemic viral pathogen.

77

## 78 **Results**

### 79 **Overexpressed IFITMs block and endogenous IFITMs boost SARS-CoV-2 infection.** It

80 has been reported that overexpression of IFITM proteins prevents entry of viral particles  
81 pseudotyped with the Spike (S) proteins of SARS- and MERS-CoVs<sup>9,11,15</sup>. In agreement with  
82 these previous findings, we found that IFITM1, IFITM2 and (less efficiently) IFITM3 dose-  
83 dependently inhibited SARS-CoV-2 S-mediated entry of Vesicular-Stomatitis-Virus  
84 pseudoparticles (VSVpp) into transfected HEK293T cells (Fig. 1a, Extended Data Fig. 1a, b).  
85 Inhibition of SARS-CoV-2 S-mediated infection by IFITM proteins was confirmed using  
86 lentiviral pseudoparticles (LVpp, Extended Data Fig. 1c). In contrast, IFITMs did not  
87 significantly affect VSV-G-dependent entry (Extended Data Fig. 1d). To examine the impact  
88 of endogenous IFITM expression on S-mediated VSVpp infection, we performed siRNA  
89 knock-down (KD) studies in the human epithelial lung cancer cell line Calu-3, which expresses  
90 ACE2<sup>16</sup> and increased levels of all three IFITM proteins upon IFN treatment (Extended Data  
91 Fig. 2a). On average, silencing of IFITM expression (Extended Data Fig. 2b) enhanced VSVpp  
92 infection mediated by SARS-CoV S proteins about 3- to 7-fold (Fig. 1b). To determine whether  
93 overexpression of IFITMs also affects genuine SARS-CoV-2 replication, we infected

94 HEK293T cells overexpressing ACE2 alone or together with individual IFITM proteins. In  
95 agreement with the inhibitory effects on S containing VSVpp and LVpp, IFITM1 and IFITM2  
96 prevented viral RNA production almost entirely, while IFITM3 achieved ~5-fold inhibition  
97 (Fig. 1c).

98 To approximate the *in vivo* situation, we also examined the role of endogenous IFITM  
99 expression on genuine SARS-CoV-2 infection of human lung cells. In striking contrast to the  
100 results obtained with pseudovirions and/or IFITM overexpression, silencing of endogenous  
101 IFITM expression in Calu-3 cells strongly impaired viral RNA production (Fig. 1d, Extended  
102 Data Fig. 2c-e). On average, IFITM2 reduced viral RNA yields by ~20-fold in the absence and  
103 by ~68-fold in the presence of IFN- $\beta$ . Consequently, the amount of infectious SARS-CoV-2  
104 particles in the cell culture supernatant was reduced by several orders of magnitude upon  
105 silencing of IFITM2 and to a lesser extent also by depletion of IFITM1 and IFITM3 (Fig. 1e).  
106 Titration analyses showed that IFITMs do not promote SARS-CoV-2 infection in transfected  
107 HEK293T cells over a broad range of expression levels (Extended Data Fig. 3). Thus, the  
108 opposing effects of transient and endogenous IFITM expression were not just due to different  
109 expression levels.

110

111 **IFITMs enhance SARS-CoV-2 infection of primary human lung cells.** To confirm that the  
112 requirement of endogenous IFITM expression for efficient SARS-CoV-2 replication is not  
113 limited to Calu-3 cells, we silenced IFITM proteins in primary small airway epithelial cells  
114 (SAEC) isolated from normal human lung tissues. Western blot analyses showed that SAEC  
115 cells express all three IFITM proteins and type I or II IFN treatment enhanced the expression  
116 levels ~2-5-fold (Fig. 2a). siRNA-mediated silencing strongly reduced the expression of IFITM  
117 proteins (Fig. 2b) and was associated with ~40- to 50-fold lower levels of SARS-CoV-2 RNA  
118 production in the presence of IFN- $\beta$  (Fig. 2c). Silencing of IFITM1 also clearly reduced viral  
119 RNA yields in the absence of IFN treatment (Fig. 2c). Altogether, IFITM1 was more critical

120 for efficient SARS-CoV-2 replication in SAEC cells than in Calu-3 cells (Figs. 1d, 2c). It is  
121 thought that IFITM1 is mainly found at the cell surface, while IFITM2 is preferentially  
122 localized in early endosomes<sup>6,7</sup>. SARS-CoV-2 may enter cells at their surface as well as in  
123 endosomes<sup>17</sup>. Thus, together with differences in the expression levels of specific IFITM  
124 proteins, cell-type-dependent differences in the major sites of viral fusion may explain  
125 differences in the relative dependency of SARS-CoV-2 on endogenous IFITM1 or IFITM2  
126 expression. In contrast to the results obtained in Calu-3 cells (Extended Data Fig. 2e), IFN- $\beta$   
127 enhanced rather than inhibited SARS-CoV-2 replication in SAEC cells (Fig. 2c). While this  
128 finding came as surprise, it is reminiscent of previous data showing that IFN treatment  
129 promotes infection by human coronavirus HCoV-OC43. Notably, this CoV was proposed to  
130 hijack IFITM3 for efficient entry<sup>18</sup>. Taken together, our results show that endogenous  
131 expression of IFITM proteins promotes SARS-CoV-2 replication in primary human lung cells,  
132 especially in the presence of IFN.

133

134 **Endogenous IFITMs promote an early step of SARS-CoV-2 infection.** To address the  
135 mechanisms underlying these opposing effects of IFITMs, we examined the effect of IFITM  
136 proteins on SARS-CoV-2 S-mediated fusion under various conditions. To analyse the impact  
137 of IFITMs on S-mediated fusion between virions and target cells, we used HIV-1 particles  
138 containing  $\beta$ -lactamase-Vpr fusions as previously described<sup>19</sup>, except that the virions contained  
139 the SARS-CoV-2 S instead of the HIV-1 Env protein. In agreement with the documented role  
140 of IFITMs as inhibitors of viral fusion<sup>12,14</sup>, transient overexpression of all three IFITM proteins  
141 blocked fusion of SARS-CoV-2 S HIVpp<sup>19</sup> with ACE2 expressing HEK293T cells (Extended  
142 Data Fig. 4a). Consistent with recent data<sup>20</sup>, results from a split-GFP assay showed that  
143 artificial overexpression of IFITMs also inhibits HEK293T cell-to-cell fusion mediated by the  
144 SARS-CoV-2 S protein and the ACE2 receptor (Extended Data Fig. 4b). To analyse the impact  
145 of endogenous IFITM expression on genuine SARS-CoV-2 entry, we determined the levels of

146 viral RNA in the cells at different time points after infection of Calu-3 cells. Already at 6 h  
147 post-infection, depletion of IFITMs 1, 2 and 3 reduced the levels of viral RNA in the cells about  
148 3-, 22- and 4-fold, respectively (Fig. 3a). At 24 h post-infection, silencing of IFITM2  
149 expression decreased intracellular SARS-CoV-2 RNA levels by 182.5-fold and extracellular  
150 viral RNA yield by 65.7-fold (Fig. 3a). These results support that in striking contrast to the  
151 overexpressed proteins, endogenous IFITM expression is required for efficient SARS-CoV-2  
152 entry into human lung cells.

153

154 **The SARS-CoV-2 Spike interacts with IFITM proteins.** It is thought that the broad-  
155 spectrum antiviral activity of IFITM proteins does not involve specific interactions with viral  
156 proteins but effects on the properties of cellular membranes<sup>5,7,21</sup>. To assess whether the ability  
157 of SARS-CoV-2 to utilize IFITMs for efficient infection of human lung cells may instead  
158 involve specific interactions between the viral S protein and IFITMs, we performed proximity  
159 ligation assays (PLA; Extended Data Fig. 5)<sup>22</sup>. The result revealed higher number of foci for S  
160 and IFITM2 compared to IFITM1 and 3 in SARS-CoV-2 infected Calu-3 cells (Fig. 3b),  
161 indicating close proximity of these two proteins. In accordance with the relevance of IFITM1  
162 for SARS-CoV-2 replication in this cell type (Fig. 2c), high levels of PLA signals were detected  
163 for S and IFITM1 in infected SAEC cells (Fig. 3b). Assessing integral membrane protein-  
164 protein interactions using the mammalian-membrane two-hybrid (MaMTH) assay<sup>23</sup> provided  
165 further evidence that SARS-CoV-2 S interacts with IFITM proteins (Fig. 2d, Extended Data  
166 Fig. 6). Finally, the SARS-CoV-2 S-protein co-immunoprecipitated IFITM2 and, to a lesser  
167 extent, IFITM1 and IFITM3 (Fig. 2e). Altogether, several independent lines of evidence  
168 support that the S protein of SARS-CoV-2 interacts with human IFITM proteins.

169

170 **Effects of endogenous IFITM expression on Spike-ACE2 interaction.** Next, we examined  
171 whether IFITMs affect the interaction between the SARS-CoV-2 S protein and the ACE2

172 receptor. Knockdown of IFITM2 and, to a lesser extent, IFITM3 enhanced the number of  
173 S/ACE2 PLA foci after infection of Calu-3 cells with genuine SARS-CoV-2 (Fig. 4a). The  
174 number of S/ACE2 foci rapidly declined (Fig. 4b) and S/RAB5A signals strongly increased  
175 (Fig. 4c) after switching SARS-CoV-2 infected Calu-3 cell cultures from ice to 37°C, most  
176 likely indicating S-mediated virion fusion in endosomes. The magnitude of these effects was  
177 reduced upon silencing of IFITM2 expression (Fig. 4d) and endogenous IFITM expression  
178 usually decreased the number of S molecules that are in close proximity to the ACE2 receptor.  
179 It is tempting to speculate that IFITMs reduce the number of S/ACE2 signals by accelerating  
180 virion fusion and hence the disappearance of signals. However, further studies are required to  
181 elucidate the details of the underlying mechanism(s).

182

183 **IFITMs are targets for inhibition of SARS-CoV-2 replication.** Our discovery that IFITMs  
184 serve as cofactors for efficient SARS-CoV-2 infection suggested that they might represent  
185 targets for viral inhibition. To address this, we examined the effect of antibodies targeting the  
186 N-terminal region of the three IFITM proteins (Fig. 5a) on SARS-CoV-2 infection of Calu-3  
187 cells. Indeed, antibodies against the N-terminal region of IFITM2 or recognizing all three  
188 IFITM proteins inhibited SARS-CoV-2 replication in Calu-3 cells up to 50-fold, while  
189 antibodies against IFITM1 or IFITM3 had negligible inhibitory effects (Fig. 5b). Since the  
190 membrane topology of IFITMs proteins is under debate<sup>7</sup>, we verified by flow cytometry  
191 analyses that the N-terminal region of IFITMs is accessible to antibody binding (Extended Data  
192 Fig. 7). Further analyses showed that peptides corresponding to the N-proximal region of  
193 IFITM2 that is recognized by inhibitory antibodies also efficiently impair SARS-CoV-2  
194 replication (Fig. 5c). In contrast, the corresponding IFITM3-derived peptide, which differs in  
195 four of the 23 residues from the IFITM2-derived peptide, and a scrambled control peptide of  
196 the same length and amino acid composition had little if any effect on viral RNA yields.  
197 Notably, incubation of SARS-CoV-2 virions with the peptides prior to infection had no

198 inhibitory effect (Extended Data Fig. 8). Thus, similarly to other inhibitors of SARS-CoV-2  
199 infection<sup>24,25</sup> the IFITM2-derived peptides might target a region in the viral S protein that only  
200 becomes accessible during the entry process.

201

202 **IFITM-derived peptides or targeting antibodies protect gut organoids and**

203 **cardiomyocytes against SARS-CoV-2.** To better assess the potential relevance of IFITMs for

204 viral spread and pathogenesis in SARS-CoV-2-infected individuals, we analysed their

205 expression in various cell types. We found that IFITM proteins are efficiently expressed in

206 primary human lung bronchial epithelial (NHBE) cells, neuronal cells, and intestinal organoids

207 derived from pluripotent stem cells (Extended Data Fig. 9a-c). These cell types and organoids

208 represent the sites of SARS-CoV-2 entry and subsequent spread, i.e. the lung and the

209 gastrointestinal tract<sup>26-28</sup>, and the potential targets responsible for neurological manifestations

210 of COVID-19<sup>29</sup>. Confocal microscopy analyses confirmed efficient induction of IFITM

211 expression by IFN- $\beta$  (Fig. 6a). NHBE cells and cultures of neuronal cells did not support

212 efficient SARS-CoV-2 replication precluding meaningful inhibition analyses. Gut organoids,

213 however, are susceptible to SARS-CoV-2 replication<sup>27</sup> and treatment with the IFITM2-derived

214 peptide or an antibody targeting the N-terminus of IFITMs strongly reduced viral RNA

215 production (Fig. 6b). Independent infection experiments confirmed that both agents

216 significantly reduce viral N protein expression and cytopathic effects in gut organoids (Fig.

217 6c). Following up on recent evidence that SARS-CoV-2 causes cardiovascular disease<sup>30</sup>, we

218 investigated viral replication in human iPSC-derived cardiomyocytes. In agreement with

219 published data<sup>31</sup>, beating cardiomyocytes were highly susceptible to viral replication (Fig. 6d).

220 All three IFITM proteins were expressed in cardiomyocytes and further induced by virus

221 infection (Fig. 6e). On average, treatment of cardiomyocytes with the IFITM2- or 3-derived

222 peptides reduced the efficiency of SARS-CoV-2 replication by ~10- and 5-fold, respectively

223 (Fig. 6f). In addition, treatment with these peptides suppressed or prevented disruptive effects

224 of virus infection on the ability of cardiomyocytes to beat in culture. Thus, IFITMs can be  
225 targeted to inhibit SARS-CoV-2 replication in cells from various human organs, including the  
226 lung, gut and heart.

227

## 228 **Discussion**

229 The present study demonstrates that endogenous expression of IFITMs is required for efficient  
230 replication of SARS-CoV-2 in human lung cells. In addition, we show that IFITMs can be  
231 targeted to inhibit SARS-CoV-2 infection of human lung, gut and heart cells. These findings  
232 came as surprise since IFITMs have been reported to inhibit SARS-CoV, MERS-CoV and,  
233 very recently, SARS-CoV-2 S-mediated infection<sup>11,15,32</sup>. Confirming and expanding these  
234 previous studies, we show that artificial overexpression of IFITM proteins in HEK293T cells  
235 prevents S-mediated VSVpp and HIVpp fusion as well as genuine SARS-CoV-2 entry.  
236 However, exactly the opposite was observed for genuine SARS-CoV-2 upon manipulation of  
237 endogenous IFITM expression in human lung cells: silencing of all three IFITM proteins  
238 reduced SARS-CoV-2 entry. Our results provide novel and highly unexpected insights into the  
239 role of IFITM proteins in the spread and pathogenesis of SARS-CoV-2 and suggest that these  
240 supposedly antiviral factors are hijacked by SARS-CoV-2 as cofactors for efficient entry.

241 While wildtype IFITM proteins have generally been described as inhibitors of SARS and  
242 MERS coronaviruses (Ref) specific point mutations may convert IFITM3 from an inhibitor to  
243 an enhancer Spike-mediated pseudoparticle transduction<sup>33</sup>. It has been reported that  
244 overexpression of IFITM3 promotes infection by hCoV-OC43, one of the causative agents of  
245 common colds<sup>18</sup>. However, IFITM3 was least relevant for SARS-CoV-2 infection in the  
246 present study. Thus, although both human coronaviruses may hijack IFITMs for efficient  
247 infection they show distinct preferences for specific IFITM proteins. It is under debate whether  
248 SARS-CoV-2 mainly fuses at the cell surface or in endosomes and cell-type-specific  
249 differences may explain why IFITM2 plays a key role in Calu-3 cells, while IFITM1 is at least

250 as important in SAEC cells. Most importantly, our results clearly demonstrate that IFITM  
251 proteins act as critical cofactors for efficient SARS-CoV-2 infection under the most  
252 physiological conditions.

253 We currently do not yet understand why overexpressed and endogenous IFITM proteins  
254 have opposite effects on SARS-CoV-2 infection. However, artificial overexpression may  
255 change the topology, localisation and endocytic activity of proteins and it has been reported  
256 that specific mutations in IFITM3 affecting these features may convert IFITM3 from an  
257 inhibitor to an enhancer of coronavirus infection<sup>9,34</sup>. The antiviral activity of IFITMs is very  
258 broad and does not involve interactions with specific viral glycoproteins<sup>6,7</sup>. In contrast, the  
259 ability of SARS-CoV-2 to hijack IFITMs for efficient entry seems to involve specific  
260 interactions between the N-terminal region of IFITMs and the viral S protein (outlined in  
261 Extended Data Fig. 10).

262 IFITMs are strongly induced during the innate immune response in SARS-CoV-2-infected  
263 individuals<sup>35,36</sup>. Thus, utilization of IFITMs as infection cofactors may promote SARS-CoV-2  
264 invasion of the lower respiratory tract as well as spread to secondary organs especially under  
265 inflammatory conditions. Further studies are required but efficient expression in neurons and  
266 cardiomyocytes suggest that IFITMs may play a role in the well documented neuronal and  
267 cardiovascular complications associated with SARS-CoV-2 infection (Ref). Perhaps most  
268 intriguingly, we show that IFITM-derived peptides and antibodies against the N-terminal  
269 region of IFITM2 efficiently inhibit SARS-CoV-2 replication. Targeting cellular IFITM  
270 proteins as a therapeutic approach should reduce the risk of viral resistance and be well  
271 tolerated since these factors are mainly known for their antiviral activity and may not exert  
272 critical physiological functions.

273

274

275

276 **Methods**

277 **Cell culture.** All cells were cultured at 37°C in a 5% CO<sub>2</sub> atmosphere. Human embryonic  
278 kidney 293T cells (HEK293T; ATCC) were maintained in Dulbecco's Modified Eagle  
279 Medium (DMEM) supplemented with 10% heat-inactivated fetal calf serum (FCS), L-  
280 glutamine (2 mM), streptomycin (100 µg/ml) and penicillin (100 U/ml). HEK293T were  
281 provided and authenticated by the ATCC. Caco-2 (human epithelial colorectal  
282 adenocarcinoma) cells were maintained in DMEM containing 10% FCS, glutamine (2 mM),  
283 streptomycin (100 µg/ml) and penicillin (100 U/ml), NEAA supplement (Non-essential amino  
284 acids (1 mM)), sodium pyruvate (1 mM). Calu-3 (human epithelial lung adenocarcinoma) cells  
285 were cultured in Minimum Essential Medium Eagle (MEM) supplemented with 10% FCS  
286 (during viral infection) or 20% (during all other times), penicillin (100 U/ml), streptomycin  
287 (100 µg/ml), sodium pyruvate (1 mM), and NEAA supplement (1 mM). Hybridoma cells  
288 (Mouse I1 Hybridoma CRL-2700; ATCC) were cultured in Roswell Park Memorial Institute  
289 (RPMI) 1640 medium supplemented with 10% FCS, L-glutamine (2 mM), streptomycin (100  
290 µg/ml) and penicillin (100 U/ml). Vero cells (ATCC, CCL-81) cells were maintained in  
291 DMEM containing 2.5% FCS, glutamine (2 mM), streptomycin (100 µg/ml) and penicillin  
292 (100 U/ml), NEAA supplement (Non-essential amino acids (1 mM)), sodium pyruvate (1 mM).  
293 Monoclonal anti-VSV-G containing supernatant was aliquoted and stored at -20°C. NHBE  
294 (primary human bronchial/tracheal epithelial, Lonza) cells were grown in Bronchial Epithelial  
295 Cell Growth Basal Medium (BEGM, Lonza) and Bronchial Epithelial Cell Growth Medium  
296 SingleQuots Supplements and Growth Factors (Lonza). SAEC (Small Airway Epithelial cells,  
297 Lonza) were grown in Small Airway Epithelial Cell Growth Basal Medium (SABM, Lonza)  
298 and Small Airway Epithelial Cell Growth Medium SingleQuots Supplements and Growth  
299 Factors (Lonza).

300

301 **Human hESC cultivation and gut organoids differentiation.** Human embryonic stem cell  
302 (hESC) line HUES8 (Harvard University) was used with permission from the Robert Koch  
303 Institute according to the “Approval according to the stem cell law” AZ 3.04.02/0084. Cells  
304 were cultured on hESC Matrigel (Corning) in mTeSR1 medium (Stemcell Technologies) at 5%  
305 CO<sub>2</sub> and 37°C. Medium was changed every day and cells were splitted twice a week with  
306 TrypLE Express (Invitrogen). Experiments involving human stem cells were approved by the  
307 Robert-Koch-Institute (Approval according to the stem cell law 29.04.2020).

308 **Cardiomyocyte differentiation.** Human episomal hiPSCs (#A18945, Thermo Fisher  
309 Scientific) at passage 2 were split using TrypLE (#12604-013, Thermo Fisher Scientific) to  
310 generate a single cell suspension. 18000 iPS cells were seeded on Geltrex (#A1413302, Thermo  
311 Fisher Scientific) matrix coated 12 well plates. 3 days post splitting differentiation protocol  
312 into iPS cardiomyocytes using the PSC cardiomyocytes Differentiation Kit (#A29212-01,  
313 Thermo) was initiated. Contracting iPSC-derived cardiomyocytes were present 14 days post  
314 differentiation initiation.

315 **Neuronal differentiation.** Human iPSC, either generated from keratinocytes as previously  
316 described<sup>37</sup> or commercially purchased from the iPSC Core facility of Cedars Sinai (Los  
317 Angeles, California), were cultured at 37°C (5% CO<sub>2</sub>, 5% O<sub>2</sub>) on Matrigel-coated (Corning,  
318 354277) 6-well plates using mTeSR1 medium (Stem Cell Technologies, 83850). Neuronal  
319 differentiation was chemically induced by culturing hiPSC colonies in suspension in ultra-low  
320 attachment T75 flasks (Corning, 3815), to allow the formation of embryoid bodies (EBs).  
321 During the first 3 days of differentiation, cells were cultivated in DMEM/F12 (Gibco, 31331-  
322 028) containing 20% knockout serum replacement (Gibco, 10828028), 1% NEAA, 1% β-  
323 mercaptoethanol, 1% antibiotic-antimycotic, SB-431542 10 μM (Stemcell Technologies,  
324 72232), Dorsomorphin 1 μM (Tocris, 3093), CHIR 99021 3 μM (Stemcell Technologies,  
325 72054), Pumorphamine 1 μM (Miltenyi Biotec, 130-104-465), Ascorbic Acid 200ng/μL,  
326 cAMP 500 μM (Sigma-Aldrich, D0260), 1% supplement (Stemcell Technologies, 05731),

327 0.5% N2 supplement (Gibco, 17502-284). From the fourth day on, medium was switched to  
328 DMEM/F12 added with 24 nM sodium selenite (Sigma-Aldrich, S5261), 16 nM progesterone  
329 (Sigma-Aldrich, P8783), 0.08 mg/mL apotransferrin (Sigma-Aldrich, T2036), 0.02 mg/mL,  
330 Insulin (Sigma-Aldrich, 91077C), 7.72 µg/mL putrescine (Sigma-Aldrich, P7505), 1%NEAA,  
331 1% antibiotic-antimycotic, 50mg/mL heparin (Sigma-Aldrich, H4783), 10 µg/mL of the  
332 neurotrophic factors BDNF (Peprotech, 450-02), GDNF (Peprotech, 450-10), and IGF1  
333 (Peprotech, 100-11), 10 µM SB-431542, 1 µM dorsomorphin, 3 µM CHIR 99021, 1 µM  
334 pumorphamine, 150 µM. vitamin C, 1 µM retinoic acid, 500 µM cAMP, 1% Neurocult  
335 supplement, 0.5% N2 supplement. After 5 further days, neurons were dissociated to single cell  
336 suspension and plated onto µDishes, or 6-well plates (Corning, 353046) pre-coated with  
337 Growth Factor Reduced Matrigel (Corning, 356231).

338 **Expression constructs.** Expression plasmids encoding for IFITM1, IFITM2 and IFITM3  
339 (pCG\_IFITM1, pCG\_IFITM2, pCG\_IFITM3 and pCG\_IFITM1-IRES\_eGFP, pCG\_IFITM2-  
340 IRES\_eGFP and pCG\_IFITM3-IRES\_BFP) were PCR amplified and subcloned in pCG based  
341 backbones using flanking restriction sites XbaI and MluI. pCG\_SARS-CoV-2-Spike-  
342 IRES\_eGFP (humanized), encoding the spike protein of SARS-CoV-2 isolate Wuhan-Hu-1,  
343 NCBI reference Sequence YP\_009724390.1 while pCG\_SARS-CoV-2-Spike C-V5-  
344 IRES\_eGFP was PCR amplified and subcloned using XbaI+MluI, while pCG\_SARS-CoV2-  
345 Spike C-V5-IRES\_eGFP was PCR amplified and subcloned using XbaI+MluI. To generate the  
346 pLV-EF1a-human ACE2-IRES-puro, pTargeT-hACE2 was provided by Sota Fukushi and  
347 Masayuki Saijo (National Institute of Infectious Diseases, Tokyo, Japan). The ORF of ACE2  
348 was extracted with MluI and SmaI and then inserted into the MluI-HpaI site of pLV-EF1a-  
349 IRES-Puro.

350 **Pseudoparticle stock production.** To produce pseudotyped VSV(luc/GFP)ΔG particles,  
351 HEK293T cells were transfected with pCG\_SARS-CoV-2-Spike C-V5-IRES\_GFP, as  
352 previously described<sup>38</sup>. 24 hours post transfection, the cells were infected with

353 VSV $\Delta$ G(GFP/luc)\*VSV-G at an MOI of 1. The inoculum was removed after 1 h. Pseudotyped  
354 particles were harvested at 16 h post infection. Cell debris was removed by centrifugation at  
355 2000 rpm for 5 min. Residual input particles carrying VSV-G were blocked by adding 10 %  
356 (v/v) of I1 Hybridoma supernatant (I1, mouse hybridoma supernatant from CRL-2700; ATCC)  
357 to the cell culture supernatant. To produce pseudotyped HIV-1(fLuc) $\Delta$ env particles, HEK293T  
358 cells were transfected with pCMVdR8.91 (Addgene) and pSEW-luc2 (Promega, # 9PIE665 )  
359 or pCMV4-BlaM-vpr (Addgene, #21950) as well as pCG\_SARS-CoV-2-Spike C-V5-  
360 IRES\_eGFP using TransIT-LT1 according to the manufacturer's protocol. Six hours post  
361 transfection, the medium was replaced with DMEM containing only 2.5% FCS. The particles  
362 were harvested 48 hours post transfection. Cell debris was pelleted by centrifugation at  
363 2000 rpm for 5 min.

364 **Target cell assay.** HEK293T cells were transiently transfected using PEI<sup>38</sup> with pLV-EF1a-  
365 human ACE2-IRES-puro and pCG-IFITM1-IRES\_eGFP or pCG-IFITM2-IRES\_eGFP or  
366 pCG-IFITM3-IRES\_BFP. 24 h post transfection, cells were transduced/infected with  
367 HIV-1 $\Delta$ env(fLuc)\* SARS-CoV-2 S or VSV(luc) $\Delta$ G\*SARS-CoV-2 S particles. 16 h post  
368 infection Luciferase activity was quantified.

369 **Luciferase assay.** To determine viral gene expression, the cells were lysed in 300 $\mu$ l of  
370 Luciferase Lysis buffer (Luciferase Cell Culture Lysis, Promega) and firefly luciferase activity  
371 was determined using the Luciferase Assay Kit (Luciferase Cell Culture, Promega) according  
372 to the manufacturer's instructions on an Orion microplate luminometer (Berthold).

373 **Vpr-BlaM fusion assay.** HEK293T cells were seeded and transiently transfected using PEI<sup>38</sup>  
374 with pLV-EF1a-human\_ACE2-IRES-puro and pCG\_IFITM1, pCG\_IFITM2 or pCG\_IFITM3.  
375 24 hours post transfection, cells were transferred to a 96-well plate. On the next day, cells were  
376 infected with 50  $\mu$ l HIV-1  $\Delta$ env (BlaM-Vpr)\*SARS-CoV-2-S particles for 2.5 h at 37  $^{\circ}$ C,  
377 followed by washing with PBS. Cells were detached and stained with CCF2/AM (1 mM) as

378 previously described<sup>39</sup>. Finally, cells were washed and fixed with 4% PFA. The change in  
379 emission fluorescence of CCF2 after cleavage by the BlaM-Vpr chimera was monitored by  
380 flow cytometry using a FACSCanto II (BD).

381 **SARS-CoV-2 virus stock production.** BetaCoV/Netherlands/01/NL/2020 or BetaCoV/  
382 France/IDF0372/2020 was propagated on Vero E6 infected at an MOI of 0.003 in serum-free  
383 medium containing 1 µg/ml trypsin as previously described<sup>16</sup>. Briefly, the cells were inoculated  
384 for 2 h at 37°C before the inoculum was removed. The supernatant was harvested 48 h post  
385 infection upon visible cytopathic effect (CPE). To remove the debris, the supernatants were  
386 centrifuged for 5 min at 1,000 × g, then aliquoted and stored at -80°C. Infectious virus titre  
387 was determined as plaque forming units (PFU).

388 **Plaque-forming Unit Assay.** The plaque-forming unit (PFU) assay was performed as  
389 previously described<sup>16</sup>. SARS-CoV-2 stocks were serially diluted and confluent monolayers of  
390 Vero E6 cells infected. After incubation for 2 h at 37°C with shaking every 20 min. The cells  
391 were overlaid with 1.5 ml of 0.8 % Avicel RC-581 (FMC) in medium and incubated for 3 days.  
392 Cells were fixed with 4 % PFA at room temperature for 45 min. After the cells were washed  
393 with PBS once 0.5 ml of staining solution (0.5 % crystal violet and 0.1 % triton in water). After  
394 20 min incubation at room temperature, the staining solution was removed using water, virus-  
395 induced plaque formation quantified, and PFU per ml calculated.

396 **qRT-PCR.** N (nucleoprotein) RNA levels were determined in supernatants or cells collected  
397 from SARS-CoV-2 infected cells 6 h, 24 h or 48 h post-infection. Total RNA was isolated  
398 using the Viral RNA Mini Kit (Qiagen) according to the manufacturer's instructions. qRT-  
399 PCR was performed according to the manufacturer's instructions using TaqMan Fast Virus 1-  
400 Step Master Mix (Thermo Fisher) and a OneStepPlus Real-Time PCR System (96-well format,  
401 fast mode). Primers were purchased from Biomers and dissolved in RNase free water.  
402 Synthetic SARS-CoV-2-RNA (Twist Bioscience) were used as a quantitative standard to

403 obtain viral copy numbers. All reactions were run in duplicates. (Forward primer (HKU-NF):  
404 5'-TAA TCA GAC AAG GAA CTG ATT A-3'; Reverse primer (HKU-NR): 5'-CGA AGG  
405 TGT GAC TTC CAT G-3'; Probe (HKU-NP): 5'-FAM-GCA AAT TGT GCA ATT TGC GG-  
406 TAMRA). GAPDH primer/probe sets (Thermo Fisher) were used for normalization of cellular  
407 RNA levels.

408 **IFITM1, 2 and 3 knock-down.** 24 h and 96 h after seeding, Calu-3 or SAEC cells were  
409 transfected twice with 20  $\mu$ M of either non-targeting siRNA or IFITM1, IFITM2 or IFITM3  
410 specific siRNA using Lipofectamine RNAiMAX (Thermo Fisher) according to the  
411 manufacturer's instructions. 14 h post transfection, medium was replaced with fresh medium  
412 supplemented with 500 U/ml IFN- $\beta$  in the indicated conditions. 7 h after the second  
413 transfection, Calu-3 or SAEC cells were infected with SARS-CoV-2 with an MOI of 0.05 and  
414 2.5 respectively. 6 h later, the inoculum was removed, cells were washed once with PBS and  
415 supplemented with fresh media. 48 h post infection, cells and supernatants were harvested for  
416 Western blot and qRT-PCR analysis respectively.

417 **Stimulation with type I interferon.** Calu-3, NHBE cells and SAEC were seeded in 12-well  
418 plates. For the gut organoids stimulation, HUES88 were seeded in 24-well-plates were coated  
419 with growth factor reduced (GFR) Matrigel (Corning) and in mTeSR1 with 10  $\mu$ M Y-27632  
420 (Stemcell technologies). The next day, differentiation to organoids was started at 80-90%  
421 confluency as previously described<sup>26</sup>. Cells or organoids were stimulated with IFN- $\alpha$ 2 (500  
422 U/ml, R&D systems 11100-1), IFN- $\beta$  (500 U/ml, R&D systems 8499-IF-010) or IFN- $\gamma$  (200  
423 U/ml, R&D systems 285-IF-100). 3 days post-stimulation whole cell lysates were generated.

424 **Cardiomyocytes infection and kinetics.** Human iPSC-derived cardiomyocytes were cultures  
425 in 12 wells plates, until they were 3 to 4 weeks old and homogenously beating. Cells were  
426 infected with increasing MOIs (0.1, 0.25, 0.5, 1, 2) of the BetaCoV/Netherlands/01/NL/2020  
427 strain. 6 h post infection, cells were washed once with PBS to remove input virus and

428 supplemented with fresh media. Virus-containing supernatant was harvested every day and  
429 replaced with fresh media until day 7 (as indicated). N gene RNA copies were determined by  
430 qRT-PCR and cells were harvested for Western blot analysis at the latest timepoint.

431 **Peptides synthesis.** The IFITM-derived peptides were synthesized by UPEP, Ulm using F-moc  
432 chemistry. Purification to homogeneity of more than 95% was done by reverse phase HPLC.  
433 Peptide stock were prepared in distilled water to a final concentration of 10 mg/ml.

434 **Inhibition by IFITM antibodies and peptides.** Calu-3 cells were seeded in 48-well format  
435 (peptides assays), or in 24-well format (antibodies assay), 24h later cells were treated with  
436 increasing concentrations (20 and 80µg/ml) of IFITMs derived peptides (human IFITM2 long:  
437 EEQEVAMLGVPHNPAPPMSTVIH, human IFITM2 short: QEVAMLGVPHNAPPMST-  
438 VIH, mouse IFITM2 long: EEYGVTELGEPSNSAVVRTTVIN, human IFITM3 long:  
439 EEHEVAVLGAPHNPAPTSTVIH, scrambled IFITM2: EGESGVTTATVEVVIERNN-  
440 LPY) or blocking antibodies (15 and 30 µg/ml) ( $\alpha$ -ACE2 AK (AC18Z), Santa Cruz  
441 Biotechnology sc-73668;  $\alpha$ -IFITM1 Cell Signaling 13126 S,  $\alpha$ -IFITM2 Cell Signaling 13530S,  
442  $\alpha$ -IFITM3 Proteintech 11714-1-AP,  $\alpha$ -IFITM1/2/3 (F-12) Santa Cruz Biotechnology sc-  
443 374026) as indicated. 2 h post-treatment, cells were infected with SARS-CoV-2 with an MOI  
444 of 0.05. 6 h post-infection, cells were washed once with PBS and supplemented with fresh  
445 MEM medium. 48 h post-infection supernatants were harvested for qRT-PCR analysis.  
446 Cardiomyocytes were seeded in 12-well plates, and treated with 100 µg/ml of indicated  
447 peptides 1h prior to infection (MOI 0.01). 6 h post infection, cells were washed once with PBS  
448 to remove input virus and supplemented with fresh media. Virus-containing supernatant was  
449 harvested every day, replaced with fresh media until day 3, and fresh peptides (100 µg/ml) (as  
450 indicated). N gene RNA copies were determined by qRT-PCR. Gut organoids were treated  
451 with increasing concentrations (15 and 30 µg/ml) of IFITMs derived peptides (mouse IFITM2  
452 antibody blocking peptide Santa Cruz sc-373676 P) and blocking antibodies ( $\alpha$ -ACE2 AK  
453 (AC18Z), Santa Cruz Biotechnology sc-73668,  $\alpha$ -IFITM1/2/3 (F-12) Santa Cruz

454 Biotechnology sc-374026) as indicated. 1h30 post-treatment, organoids were infected with  
455 SARS-CoV-2 with an MOI 0.15 as previously described<sup>40</sup>. 48 h post-infection gut organoids  
456 were harvested for qRT-PCR analysis.

457 **Virus treatment.** Calu-3 cells were seeded in 48-wells, 24 h later SARS-COV-2 (0.05 MOI)  
458 was incubated for 30 min at 37°C with indicated concentrations of IFITM-derived peptides. 50  
459 µl of the inoculum were used to infect the cells. 6h later cells were supplemented with fresh  
460 medium. 48 h post-infection supernatants were harvested for qRT-PCR analysis.

461 **Flow cytometry analysis of IFITMs.** HEK293T cells were transfected with pCG\_IFITM1, 2  
462 or 3 using PEI as previously described. Calu-3 cells were seeded 24 h before harvest in a 6 well  
463 format. 24h post transfection and post seeding, cells were harvested using a scraper and stained  
464 with the eBioscience Fixable Viability Dye eFluor 780 (Thermo Fisher) for 15 minutes at room  
465 temperature in the dark. Afterwards cells were washed three times with PBS and fixed with  
466 100µl of Reagent A (FIX & PERM Fixation and Permeabilization Kit, Nordic MUBio) for 30  
467 minutes at room temperature, washed three time with PBS and stained with primary antibody  
468 ( $\alpha$ -IFITM1 Cell Signaling 13126 S,  $\alpha$ -IFITM2 Cell Signaling 13530S,  $\alpha$ -IFITM3 Proteintech  
469 11714-1-AP,  $\alpha$ -IFITM1/2/3 (F-12) Santa Cruz Biotechnology sc-374026,) diluted 1:20 in PBS  
470 or in Reagent B (FIX & PERM Fixation and Permeabilization Kit Nordic MUBio) for 1 h at  
471 4°C. Cells were washed three times with PBS and stained with secondary antibody (Goat Anti-  
472 Rabbit IgG H&L (PE), ab72465, Donkey Anti-Mouse IgG H&L (PE) ab7003, 1:50) for 1 h at  
473 4°C. After several washing with PBS, cells were resuspended in 100µl of PBS.

474 **Immunofluorescence of gut organoids.** For histological examination, organoids were fixed  
475 in 4 % PFA over night at 4°C, washed with PBS, and pre-embedded in 2 % agarose (Sigma) in  
476 PBS. After serial dehydration, intestinal organoids were embedded in paraffin, sectioned at 4  
477 µm, deparaffinized, rehydrated and subjected to heat mediated antigen retrieval in tris Buffer  
478 (pH 9) or citrate buffer (pH 6). Sections were permeabilized with 0.5 % Triton-X for 30 min at

479 RT and stained over night with primary antibodies (rabbit anti-IFITM1 Cell Signaling 13126  
480 S, 1:500 or rabbit anti-IFITM2 Cell Signaling #13530S, 1:500 or rabbit anti-IFITM3 Cell  
481 Signaling #59212S, 1:250 or anti-SARS-CoV-2 N 1:500 or anti-E-Cadherin 1:500) diluted in  
482 antibody diluent (Zytomed) in a wet chamber at 4°C. After washing with PBS-Tween 20, slides  
483 were incubated with secondary antibodies (Alexa Fluor IgG H+L, Invitrogen, 1:500) and 500  
484 ng/ml DAPI in Antibody Diluent for 90 min in a wet chamber at RT. After washing with PBS-  
485 T and water, slides were mounted with Fluoromount-G (Southern Biotech). Negative controls  
486 were performed using IgG controls or irrelevant polyclonal serum for polyclonal antibodies,  
487 respectively. Cell borders were visualized by E-cadherin staining. Images were acquired using  
488 a LSM 710 system.

489 **GFP Split fusion assay.** GFP1-10 and GFP11-expressing HEK293T cells were seeded  
490 separately in a 24-well plate. One day post seeding, cells were transiently transfected using the  
491 calcium-phosphate precipitation method<sup>41</sup>. GFP1-10 cells were co-transfected with increasing  
492 amounts (0, 8, 16, 32, 64, 125, 250, 500 ng) of pCG\_IFTM1, pCG\_IFITM2, pCG\_IFITM3 and  
493 250 ng of pLV-EF1a-human ACE2-IRES-puro. GFP11 cells were transfected with 250 ng of  
494 pCG\_SARS-CoV-2-Spike C-V5 codon optimised. 16 h post transfection, GFP1-10 and GFP11  
495 cells were co-cultured in poly-L-lysine-coated 24-well plate. 24 h post co-culturing, cells were  
496 fixed with 4 % PFA and cell nuclei were stained using NucRed Live 647 ReadyProbes Reagent  
497 (Invitrogen) according to the manufacturer's instructions. Fluorescence imaging of GFP and  
498 NucRed was performed using a Cytation3 imaging reader (BioTek Instruments). 12 images per  
499 well were recorded automatically using the NucRed signal for autofocusing. The GFP area was  
500 quantified using ImageJ.

501 **Whole cell lysates.** To determine expression of cellular and viral proteins, cells were washed  
502 in PBS and subsequently lysed in Western blot lysis buffer (150 mM NaCl, 50 mM HEPES,  
503 5 mM EDTA, 0.1% NP40, 500 µM Na<sub>3</sub>VO<sub>4</sub>, 500 µM NaF, pH 7.5) supplemented with protease  
504 inhibitor (1:500, Roche) as previously described<sup>38</sup>. After 5 min of incubation on ice, samples

505 were centrifuged (4°C, 20 min, 14.000 rpm) to remove cell debris. The supernatant was  
506 transferred to a fresh tube, the protein concentration was measured and adjusted using Western  
507 blot lysis buffer. Lysates from iPSC-derived neurons were prepared following previously  
508 published protocols<sup>42</sup>. Briefly, neurons were harvested in cold PBS (Gibco) and centrifuged at  
509 5000 RPM for 3 minutes. Pellets were then resuspended and incubated at 4°C on an orbital  
510 shaker for 2 hours in RIPA buffer. Lysate were then sonicated and protein concentration was  
511 determined by Bradford assay.

512 **SDS-PAGE and Immunoblotting.** Western blotting was performed as previously described<sup>38</sup>.  
513 In brief, whole cell lysates were mixed with 4x or 6x Protein Sample Loading Buffer (LI-COR,  
514 at a final dilution of 1x) supplemented with 10 %  $\beta$ -mercaptoethanol (Sigma Aldrich), heated  
515 at 95°C for 5 min, separated on NuPAGE 4 $\pm$ 12% Bis-Tris Gels (Invitrogen) for 90 minutes at  
516 100 V and blotted onto Immobilon-FL PVDF membranes (Merck Millipore). The transfer was  
517 performed at a constant voltage of 30 V for 30 minutes. After the transfer, the membrane was  
518 blocked in 1 % Casein in PBS (Thermo Scientific). Proteins were stained using primary  
519 antibodies against IFITM1 ( $\alpha$ -IFITM1, Cell Signaling #13126 S, 1:1000), IFITM2 ( $\alpha$ -IFITM2  
520 Cell Signaling #13530S, 1:1000), IFITM3 ( $\alpha$ -IFITM3 Cell Signaling #59212S, 1:1000) SARS  
521 Spike CoV-2 (SARS-CoV-1/-2 (COVID-19) spike antibody [1A9], GTX-GTX632604,  
522 1:1000), VSV-M (Mouse Monoclonal Anti-VSV-M Absolute antibody, ABAAb01404-21.0,  
523 1:1000), actin (Anti-beta Actin antibody Abcam, ab8227, 1:5000 Abcam), ACE2 (Rabbit  
524 polyclonal anti-ACE2 Abcam, ab166755, 1:1000) and Infrared Dye labelled secondary  
525 antibodies (LI-COR IRDye). Membranes were scanned using LI-COR and band intensities  
526 were quantified using Image Studio (LI-COR).

527 **Proximity Ligation Assay.** The proximity ligation assay (PLA) was performed as previously  
528 described<sup>43</sup>. In brief, Calu-3 or SAEC were seeded in a 24-well plate on a cover slip glass. 24 h  
529 and 72 h post seeding, the cells were transfected with 20  $\mu$ M either non-targeting siRNA or  
530 IFITM1 or IFITM3 siRNAs using RNAimax according to the manufacturer's instructions.

531 Prior infection, cells were pre-chilled for 30 minutes at 4°C and then infected with  
532 VSV(luc) $\Delta$ G\*-SARS-CoV-2 S (MOI 2) or BetaCoV/France/IDF0372/2020 (MOI 0.05) for 2  
533 h on ice. Cells have been washed once with cold PBS and fixed with 4% PFA. For staining  
534 following antibodies were used: IFITM1 ( $\alpha$ -IFITM1 Cell Signaling 13126 S), IFITM2 ( $\alpha$ -  
535 IFITM2 Abcam 236735), IFITM3 ( $\alpha$ -IFITM3 Cell Signaling 59212S), SARS Spike CoV-2  
536 (SARS-CoV / SARS-CoV-2 (COVID-19) spike antibody [1A9], GTX-GTX632604), Rab5  
537 alpha (Rab5 (RAB5A) Goat Polyclonal Antibody Origene AB0009-200) and ACE2 (Rabbit  
538 polyclonal anti-ACE2 Abcam, ab166755). All in a concentration 1:100. Images were acquired  
539 on a Zeiss LSM 710 and processed using ImageJ (Fiji).

540 **Co-immunoprecipitation SARS-CoV-2 Spike and IFITMs.** HEK293Ts were transfected  
541 using PEI with 0.5  $\mu$ g pCG-SARS CoV2 Spike-V5 and 0.5  $\mu$ g of pCG IFITM1, IFITM2 or  
542 IFITM3. 24 h later, samples were lysed with IP lysis buffer (50 mM, Tris pH8, 150 mM NaCl,  
543 1 % NP40, protease inhibitor) for 10 min on ice. Lysed samples were centrifuged and incubated  
544 for 3 h with Pierce Protein A/G Magnetic beads (88802) which were pre-incubated over night  
545 with V5 antibody (Cell signaling E9H80; 5  $\mu$ g of primary antibody per 10  $\mu$ l of beads per  
546 sample).

547 **MaMTH assay.** Human IFITM proteins and SARS-CoV-2 viral proteins were cloned into  
548 MaMTH N-term tagged Prey and C-term tagged Bait vectors respectively using Gateway  
549 cloning technology (ThermoFisher). Correctness of recombined insertions was confirmed by  
550 Sanger sequencing (Eurofins). The Mammalian Membrane Two-Hybrid (MaMTH) Assay has  
551 been performed as previously described<sup>23,44</sup>. HEK293T B0166 Gaussia luciferase reporter cells  
552 were co-transfected in 96-well plates with 25 ng SARS-CoV-2 protein Bait and 25 ng IFITM  
553 or control protein Prey MaMTH vectors in triplicates using PEI transfection reagent. Gal4  
554 (transcription factor) as well as EGFR Bait with SHC1 Prey served as positive controls,  
555 whereas SARS-CoV-2 Bait proteins with Pex7 Prey were used as negative controls. The  
556 following day, Bait protein expression was induced with 0.1 $\mu$ g/ml doxycycline. Cell-free

557 supernatants were harvested 2 days post-transfection and the released Gaussia reporter was  
558 measured 1 s after injecting 20 mM coelenterazine substrate using an Orion microplate  
559 luminometer. To determine the level of protein interaction, Gaussia values were normalized to  
560 Pex7 Prey negative control for each Bait. To determine Bait and Prey protein expression levels,  
561 HEK293T B0166 transfected and treated in the same manner were harvested two days post-  
562 transfection and lysed in Co-IP buffer (150 mM NaCl, 50 mM HEPES, 5 mM EDTA, 0.10%  
563 NP40, 0.5 mM sodium orthovanadate, 0.5 mM NaF, protease inhibitor cocktail from Roche)  
564 and reduced in the presence of  $\beta$ -mercaptoethanol by boiling at 95°C for 10 min. Proteins were  
565 separated in 4 to 12% Bis-Tris gradient acrylamide gels (Invitrogen), blotted onto  
566 polyvinylidene difluoride (PVDF) membrane, blocked in 5% milk and probed with rabbit anti-  
567 V5 (Cell Signaling #13202), mouse anti-FLAG (Sigma #F1804) and rat anti-GAPDH  
568 (Biolegend #607902) antibodies, followed by goat anti-mouse, anti-rabbit and anti-rat  
569 secondary fluorescent antibodies (LI-COR). Membranes were scanned with LI-COR Odyssey  
570 reader.

571 **Statistics.** Statistical analyses were performed using GraphPad PRISM 8 (GraphPad Software).  
572 P-values were determined using a two-tailed Student's t test with Welch's correction. Unless  
573 otherwise stated, data are shown as the mean of at least three independent experiments  $\pm$  SEM.  
574 Significant differences are indicated as: \*,  $p < 0.05$ ; \*\*,  $p < 0.01$ ; \*\*\*,  $p < 0.001$ . Statistical  
575 parameters are specified in the figure legends.

576 **References**

- 577 1. Ksiazek, T. G. *et al.* A novel coronavirus associated with severe acute respiratory  
578 syndrome. *New England Journal of Medicine* **348**, 1953–1966 (2003).
- 579 2. Bermingham, A. *et al.* Severe respiratory illness caused by a novel coronavirus, in a  
580 patient transferred to the United Kingdom from the Middle East, September 2012.  
581 *Eurosurveillance* **17**, (2012).
- 582 3. Al-Rohaimi, A. H. & Al Otaibi, F. Novel SARS-CoV-2 outbreak and COVID19  
583 disease; a systemic review on the global pandemic. *Genes Dis* **7**, 491–501 (2020).
- 584 4. Sa Ribero, M., Jouvenet, N., Dreux, M. & Nisole, S. Interplay between SARS-CoV-2  
585 and the type I interferon response. *PLoS pathogens* **16**, e1008737 (2020).
- 586 5. Zhao, X., Li, J., Winkler, C. A., An, P. & Guo, J. T. IFITM genes, variants, and their  
587 roles in the control and pathogenesis of viral infections. *Frontiers in Microbiology* vol. 10  
588 (2019).
- 589 6. Diamond, M. S. & Farzan, M. The broad-spectrum antiviral functions of IFIT and  
590 IFITM proteins. *Nature Reviews Immunology* vol. 13 46–57 (2013).
- 591 7. Bailey, C. C., Zhong, G., Huang, I.-C. & Farzan, M. IFITM-Family Proteins: The  
592 Cell’s First Line of Antiviral Defense. *Annual Review of Virology* **1**, 261–283 (2014).
- 593 8. Ferreira, J. M., Chin, C. R., Feeley, E. M. & Brass, A. L. *IFITMs restrict the*  
594 *replication of multiple pathogenic viruses*. *Journal of Molecular Biology* vol. 425 (Academic  
595 Press, 2013).
- 596 9. Shi, G. *et al.* Opposing activities of IFITM proteins in SARS-CoV-2 infection. *EMBO*  
597 *J* e106501 (2020) doi:10.15252/embj.2020106501.
- 598 10. Smith, S. E., Weston, S., Kellam, P. & Marsh, M. *IFITM proteins - Cellular*  
599 *inhibitors of viral entry*. *Current Opinion in Virology* vol. 4 (Elsevier B.V., 2014).
- 600 11. Huang, I. C. *et al.* Distinct patterns of IFITM-mediated restriction of filoviruses,  
601 SARS coronavirus, and influenza A virus. *PLoS Pathogens* **7**, (2011).
- 602 12. Zani, A. & Yount, J. S. Antiviral Protection by IFITM3 In Vivo. *Current Clinical*  
603 *Microbiology Reports* vol. 5 229–237 (2018).
- 604 13. Li, K. *et al.* IFITM Proteins Restrict Viral Membrane Hemifusion. *PLoS Pathogens* **9**,  
605 (2013).
- 606 14. Shi, G., Schwartz, O. & Compton, A. A. More than meets the I: The diverse antiviral  
607 and cellular functions of interferon-induced transmembrane proteins. *Retrovirology* vol. 14  
608 (2017).
- 609 15. Wrensch, F., Winkler, M. & Pöhlmann, S. IFITM proteins inhibit entry driven by the  
610 MERS-Coronavirus Spike protein: Evidence for Cholesterol-Independent Mechanisms.  
611 *Viruses* **6**, 3683–3698 (2014).
- 612 16. Nchioua, R. *et al.* SARS-CoV-2 Is Restricted by Zinc Finger Antiviral Protein despite  
613 Preadaptation to the Low-CpG Environment in Humans. *mBio* **11**, 16 (2020).

- 614 17. Shang, J. *et al.* Cell entry mechanisms of SARS-CoV-2. *PNAS* **117**, 11727–11734  
615 (2020).
- 616 18. Zhao, X. *et al.* Interferon induction of IFITM proteins promotes infection by human  
617 coronavirus OC43. *Proceedings of the National Academy of Sciences of the United States of*  
618 *America* **111**, 6756–6761 (2014).
- 619 19. Cavrois, M., De Noronha, C. & Greene, W. C. A sensitive and specific enzyme-based  
620 assay detecting HIV-1 virion fusion in primary T lymphocytes. *Nature biotechnology* **20**,  
621 1151–4 (2002).
- 622 20. Buchrieser, J. *et al.* Syncytia formation by SARS-CoV-2-infected cells. *EMBO J* **39**,  
623 e106267 (2020).
- 624 21. Yáñez, D. C., Ross, S. & Crompton, T. *The IFITM protein family in adaptive*  
625 *immunity*. *Immunology* vol. 159 (Blackwell Publishing Ltd, 2020).
- 626 22. Hampp, S. *et al.* DNA damage tolerance pathway involving DNA polymerase  $\eta$  and  
627 the tumor suppressor p53 regulates DNA replication fork progression. *Proceedings of the*  
628 *National Academy of Sciences* **113**, E4311–E4319 (2016).
- 629 23. Petschnigg, J. *et al.* The mammalian-membrane two-hybrid assay (MaMTH) for  
630 probing membrane-protein interactions in human cells. *Nature Methods* **11**, 585–592 (2014).
- 631 24. Schütz, D. *et al.* Peptide and peptide-based inhibitors of SARS-CoV-2 entry. *Adv*  
632 *Drug Deliv Rev* **167**, 47–65 (2020).
- 633 25. Xia, S. *et al.* Inhibition of SARS-CoV-2 (previously 2019-nCoV) infection by a  
634 highly potent pan-coronavirus fusion inhibitor targeting its spike protein that harbors a high  
635 capacity to mediate membrane fusion. *Cell Res* **30**, 343–355 (2020).
- 636 26. Krüger, J. *et al.* Remdesivir but not famotidine inhibits SARS-CoV-2 replication in  
637 human pluripotent stem cell-derived intestinal organoids. *bioRxiv* 2020.06.10.144816 (2020)  
638 doi:10.1101/2020.06.10.144816.
- 639 27. Lamers, M. M. *et al.* SARS-CoV-2 productively infects human gut enterocytes.  
640 *Science (New York, N.Y.)* **369**, 50–54 (2020).
- 641 28. Hoffmann, M. *et al.* SARS-CoV-2 Cell Entry Depends on ACE2 and TMPRSS2 and  
642 Is Blocked by a Clinically Proven Protease Inhibitor. *Cell* (2020)  
643 doi:10.1016/j.cell.2020.02.052.
- 644 29. Ramani, A. *et al.* SARS-CoV-2 targets neurons of 3D human brain  
645 organoids. *The EMBO Journal* **39**, (2020).
- 646 30. Magadum, A. & Kishore, R. Cardiovascular Manifestations of COVID-19 Infection.  
647 *Cells* **9**, (2020).
- 648 31. Bojkova, D. *et al.* SARS-CoV-2 infects and induces cytotoxic effects in human  
649 cardiomyocytes. *Cardiovasc Res* **116**, 2207–2215 (2020).
- 650 32. Shi, G. *et al.* Opposing activities of IFITM proteins in SARS-CoV-2 infection.  
651 *bioRxiv* 2020.08.11.246678 (2020) doi:10.1101/2020.08.11.246678.

- 652 33. Zhao, X. *et al.* Identification of Residues Controlling Restriction versus Enhancing  
653 Activities of IFITM Proteins on Entry of Human Coronaviruses. *Journal of Virology* **92**,  
654 (2017).
- 655 34. Zhao, X. *et al.* Identification of Residues Controlling Restriction versus Enhancing  
656 Activities of IFITM Proteins on Entry of Human Coronaviruses. *Journal of Virology* **92**,  
657 (2017).
- 658 35. Blanco-Melo, D. *et al.* Imbalanced host response to SARS-CoV-2 drives development  
659 of COVID-19. *Cell* (2020) doi:10.1016/j.cell.2020.04.026.
- 660 36. Hadjadj, J. *et al.* Impaired type I interferon activity and inflammatory responses in  
661 severe COVID-19 patients. *Science (New York, N.Y.)* (2020) doi:10.1126/science.abc6027.
- 662 37. Linta, L., Boeckers, T. M., Kleger, A. & Liebau, S. Calcium activated potassium  
663 channel expression during human iPS cell-derived neurogenesis. *Ann Anat* **195**, 303–311  
664 (2013).
- 665 38. Koepke, L. *et al.* An improved method for high-throughput quantification of  
666 autophagy in mammalian cells. *Scientific Reports* **10**, 1–20 (2020).
- 667 39. Cavrois, M., De Noronha, C. & Greene, W. C. A sensitive and specific enzyme-based  
668 assay detecting HIV-1 virion fusion in primary T lymphocytes. *Nature Biotechnology* (2002)  
669 doi:10.1038/nbt745.
- 670 40. Krüger, J. *et al.* Drug Inhibition of SARS-CoV-2 Replication in Human Pluripotent  
671 Stem Cell-Derived Intestinal Organoids. *Cell Mol Gastroenterol Hepatol* (2020)  
672 doi:10.1016/j.jcmgh.2020.11.003.
- 673 41. Chen, C. & Okayama, H. High-efficiency transformation of mammalian cells by  
674 plasmid DNA. *Molecular and Cellular Biology* **7**, 2745–2752 (1987).
- 675 42. Catanese, A. *et al.* Retinoic acid worsens ATG10-dependent autophagy impairment in  
676 TBK1-mutant hiPSC-derived motoneurons through SQSTM1/p62 accumulation. *Autophagy*  
677 **15**, 1719–1737 (2019).
- 678 43. Volcic, M. *et al.* Vpu modulates DNA repair to suppress innate sensing and hyper-  
679 integration of HIV-1. *Nature Microbiology* (2020) doi:10.1038/s41564-020-0753-6.
- 680 44. Kmiec, D. *et al.* SIVcol Nef counteracts SERINC5 by promoting its proteasomal  
681 degradation but does not efficiently enhance HIV-1 replication in human CD4+ T cells and  
682 lymphoid tissue. *PLOS Pathogens* **14**, e1007269 (2018).
- 683 45. He, S. *et al.* *PSGL-1 blocks SARS-CoV-2 S protein-mediated virus attachment and*  
684 *infection of target cells.* *bioRxiv : the preprint server for biology* (Cold Spring Harbor  
685 Laboratory, 2020). doi:10.1101/2020.05.01.073387.
- 686
- 687

688 **Acknowledgments.** We thank K. Regensburger, S. Engelhart, M. Meyer, R. Burger, N.  
689 Schrott, N. Preising and D. Krnavek for technical assistance and. The ACE2 vector and the  
690 SARS-CoV-2 S-HA plasmid were provided by Shinji Makino and Stefan Pöhlmann. We thank  
691 K-K. Conzelmann for providing VSVΔG and the Core Functional Peptidomics of Ulm  
692 University for peptide synthesis. This study was supported by DFG grants to F.K., J.Mün.,  
693 D.K., K.M.J.S., D.Sa. (CRC 1279, SPP 1923, KM 5/1-1, SP1600/4-1), C.G. (GO2153/3-1)  
694 EU's Horizon 2020 research and innovation program to J.M. (Fight-nCoV, 101003555), as  
695 well as the BMBF to F.K., D.Sa. and K.M.J.S. (Restrict SARS-CoV-2, protACT and  
696 IMMUNOMOD). C.P.B., C.C., and R.G. are part of and R.G. is funded by a scholarship from  
697 the International Graduate School in Molecular Medicine Ulm (IGradU).

698 **Author Contributions.** C.P.B. and R.N. performed most experiments. M.V. performed  
699 interaction assays. J.K., S.H. and A.K. provided gut organoids. C.M.S. generated most  
700 expression constructs. D.K. performed MaMTH assays. J. Mül., C.C. and J. Mün provided  
701 SARS-CoV-2. F.Z. assisted in experiments with infectious SARS-CoV-2. L.W., T.W. and R.G.  
702 provided reagents and protocols. D.Sc. performed FACS for the Vpr-BlaM assay; E.B. and  
703 J.W. performed the HEK293T GFP split fusion assay. L.K. helped with the microscopy  
704 analysis of organoids. F.D. and S.J. provided cardiomyocytes. A.C. M.S. and T.B. provided  
705 neurons. D.S., C.G., S.S. and J. Mün. provided comments and resources. K.M.J.S and F.K.  
706 conceived the study, planned experiments and wrote the manuscript. All authors reviewed and  
707 approved the manuscript.

708 **Competing interests.** The authors declare no competing interests.

709 **Data Availability.** The datasets generated during and/or analyzed during the current study  
710 are available from the corresponding authors on request.

711 **Figure legends**

712 **Fig. 1 | Opposing effects of IFITM proteins on SARS-CoV-2 infection.** **a**, Quantification of  
713 VSV(luc) $\Delta$ G\*SARS-CoV-2-S entry by measuring luciferase activity in HEK293T cells  
714 transiently expressing the indicated IFITM proteins. Bars in all panels show results of three  
715 independent experiments (mean value,  $\pm$ SEM). **b**, Calu-3 cells treated with non-targeting  
716 (CTRL) or IFITM1, 2 or 3 siRNAs or a combination of the three and infected with  
717 VSV(luc) $\Delta$ G\*SARS-CoV-2-S particles. **c**, Quantification of RNA containing N gene  
718 sequences by qRT-PCR in the supernatant of HEK293T cells transiently expressing ACE2  
719 alone or together with the indicated IFITM proteins 48 h post-infection with SARS-CoV-2  
720 (MOI 0.05). **d**, RNA containing N gene sequences levels in the supernatant of Calu-3 cells,  
721 collected 48 h post-infection with SARS-CoV-2 (MOI 0.05). Cells were transfected with  
722 control (CTRL) or IFITM1, 2 and/or 3 targeting siRNA or a combination of the three and either  
723 treated with IFN- $\beta$  or left untreated as indicated. **e**, Cytopathic effects in Vero cells infected  
724 with serial dilutions of Calu-3 supernatants from Figure 1d. Cells were stained with crystal  
725 violet.

726 **Fig. 2 | Role of IFITMs in SARS-CoV-2 replication in SAEC.** **a**, Expression of IFITM1,  
727 IFITM2 and IFITM3 in SAEC after stimulation with IFN- $\alpha$ 2 (500 U/ml, 72 h), IFN- $\beta$  (500  
728 U/ml, 72 h) or IFN- $\gamma$  (200 U/ml, 72 h). Immunoblots of whole cell lysates were stained with  
729 anti-IFITM1, anti-IFITM2, anti-IFITM3 and anti-GAPDH. **b**, Expression of IFITM proteins in  
730 SAEC treated with non-targeting or IFITM specific siRNAs. Cells were either stimulated with  
731 IFN- $\beta$  (500 U/ml, 72 h) or left untreated. Immunoblots of whole cell lysates were stained with  
732 anti-IFITM1, anti-IFITM2, anti-IFITM3 and anti-GAPDH. **c**, SARS-CoV-2 N quantification  
733 in the supernatant of SAEC 2 days post-infection with SARS-CoV-2 (MOI 2.5).

734 **Fig. 3 | IFITM2 promotes SARS-CoV-2 entry and interacts with the Spike protein.** **a**,  
735 Intracellular RNA containing N gene sequences copy numbers in Calu-3 cells 6 h (left) and 24  
736 h (middle) post-infection with SARS-CoV-2 (MOI 0.05). Values were normalized to GAPDH

737 and calculated relative to the control (set to 100%). The right panel shows viral RNA copies in  
738 the cell culture supernatant at 24 h post infection. Cells were transiently transfected with siRNA  
739 either control (CTRL) or targeting IFITM1, 2, 3, or a combination of the three as indicated.  
740 Bars represent n=1, measured in duplicates,  $\pm$ SD. **b**, Proximity ligation assay between the  
741 SARS-CoV-2 Spike and IFITM proteins in Calu-3 cells infected with SARS-CoV-2 for 2 h at  
742 4°C. DAPI (blue), nuclei. PLA signal (yellow), proximity between S/IFITMs. Results represent  
743 two independent experiments done in technical duplicates. **c**, PLA in SAEC. Bars represent  
744 means of n=1 (45-70 cells)  $\pm$ SEM. DAPI (blue), nuclei. PLA signal (yellow), proximity  
745 between S/IFITMs. Scale bar, 20  $\mu$ m. **d**, Relative interaction between SARS-CoV-2 Spike and  
746 human IFITM proteins measured by MaMTH protein-protein interaction assay in cotransfected  
747 HEK293T B0166 *Gaussia* luciferase reporter cells. Bars represent the mean of triplicate  
748 transfections performed in two independent experiments. **e**, Immunoprecipitation of IFITM  
749 proteins by the Spike protein. HEK293T cells were transfected with or without a construct to  
750 overexpress SARS-CoV-2 S (indicated with a + or a -) and IFITM1, IFITM2 or IFITM3. 24 h  
751 post transfection, cells were harvested and SARS-CoV-2 Spike was immunoprecipitated.  
752 WCL, whole cell lysates.

753 **Fig. 4 | Impact of IFITMs on the ACE2-SARS-CoV-2 S proximity.** **a**, PLA between SARS-  
754 CoV-2 Spike and ACE2 in Calu-3 depleted of IFITM1, IFITM2 or IFITM3 and infected with  
755 genuine SARS-CoV-2. Lines represent means of n=2 (a) n=3 (b) (60-100 cells)  $\pm$ SEM. **b**, PLA  
756 between Spike and ACE2 in Calu-3 cells depleted of IFITM2 and infected with SARS-CoV-2  
757 virus on ice for 2 h and then incubated for 15 min at 37°C. Lines represent means of n=3 (200-  
758 300 cells)  $\pm$ SEM. **c**, PLA assay between Spike and RAB5A in Calu-3 cells infected as in **c**.  
759 Lines represent means of n=2 (130-200 cells)  $\pm$ SEM. DAPI (blue), nuclei. PLA signal (yellow).  
760 Scale bar, 20  $\mu$ m. **d**, Quantification of ACE2-Spike and Spike-RAB5 alpha proximity upon  
761 SARS-CoV-2 infection.

762 **Fig. 5 | IFITM blocking antibodies and IFITM derived peptides target the N-terminal**  
763 **domain. a**, Alignment of the amino acid sequence of human IFITM1, 2 and 3. Binding sites  
764 of IFITM blocking antibodies are indicated and the region of origin of the IFITM derived  
765 peptides highlighted. **b**, Viral N gene RNA levels in the supernatant of Calu-3 cells treated with  
766  $\alpha$ -ACE2,  $\alpha$ -IFITM1,  $\alpha$ -IFITM2,  $\alpha$ -IFITM3 and  $\alpha$ -IFITM1-3 antibodies, collected 48 h post  
767 infection (MOI 0.05). Bars represent one to two independent experiments each measured in  
768 technical duplicates (mean value,  $\pm$ SEM). **c**, RNA containing N gene sequences in the  
769 supernatant of Calu-3 cells treated with IFITM-derived peptides, collected 48 h post infection  
770 (MOI 0.05). Bars represent two to three independent experiments each measured in technical  
771 duplicates (mean value,  $\pm$ SEM).

772 **Fig. 6 | Blocking antibodies and IFITM-derived peptides treatment decrease SARS-CoV-**  
773 **2 infection in gut organoids and cardiomyocytes. a**, Immunofluorescence images of stem  
774 cell-derived gut organoids after stimulation with IFN- $\beta$  (500 U/ml, 72 h) **b**, Cell-associated  
775 viral N gene RNA copy numbers in organoids treated with  $\alpha$ -ACE2, mIFITM2 antibody  
776 blocking peptide and  $\alpha$ -IFITM1-3 and infected with SARS-CoV-2 (MOI 0.15).**c**,  
777 Immunohistochemistry of gut organoids treated as in **e** and infected with SARS-CoV-2 (MOI  
778 0.5). Organoids were stained with anti SARS-CoV-2 N (red), E-Cadherin (green) and DAPI  
779 (blue). Scale bar, 100  $\mu$ m (left panel). SARS-CoV-2 N quantification of infected gut organoids  
780 treated as in **e** (right panel). **d**, Viral N gene RNA levels in the supernatant of SARS-CoV-2  
781 infected cardiomyocytes (increasing MOIs as indicated), virus containing supernatants at  
782 indicated timepoints. **e**, Expression of IFITM1, IFITM2 and IFITM3 in cardiomyocytes  
783 infected with SARS-CoV-2. Immunoblot of whole cell lysates stained with anti-IFITM1, anti-  
784 IFITM2, anti-IFITM3 and anti-GAPDH **f**, Viral N gene RNA levels in the supernatant of  
785 SARS-CoV-2 infected cardiomyocytes (0.05 MOI) treated with IFITM-derived peptides,  
786 collected at indicated timepoints post infection. Bars represent two independent experiments  
787 each measured in technical duplicates (mean value,  $\pm$ SEM). bql, below quantification level.

# Figure 1

Pirelli Bozzo, Nchioua *et al.*

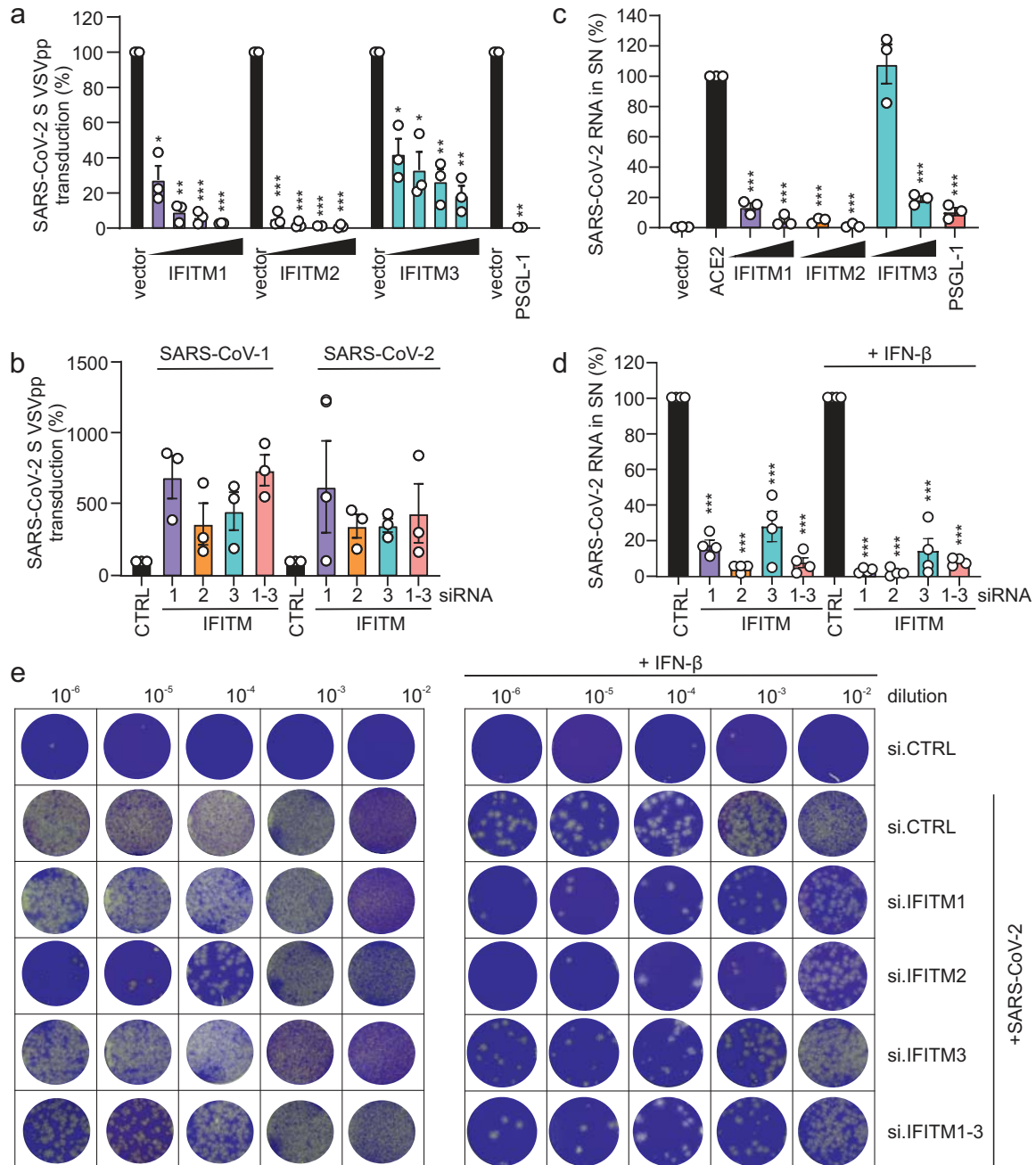


## Figure 2

Prelli Bozzo, Nchioua *et al.*

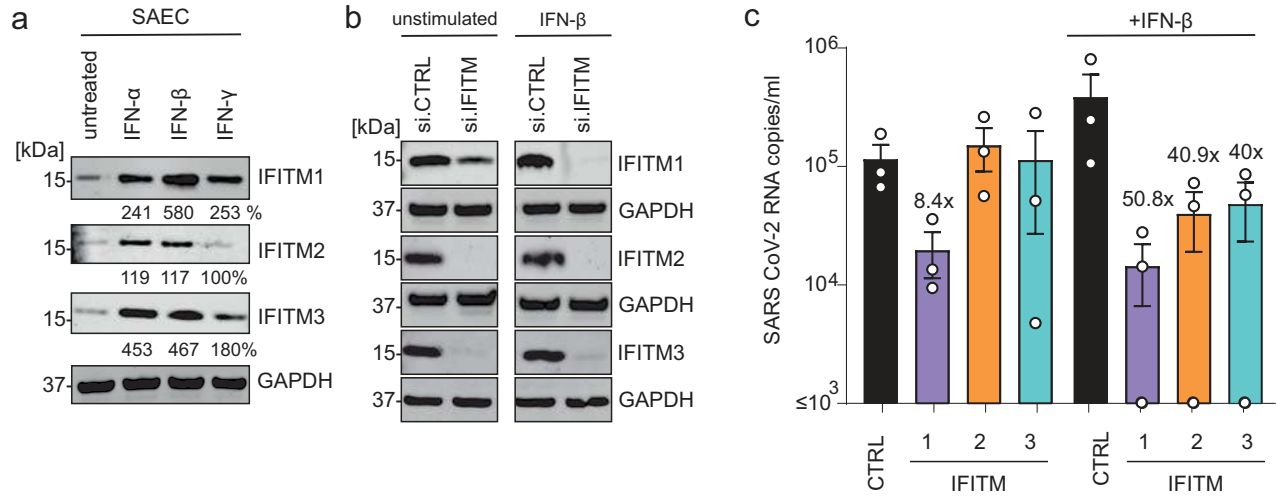


# Figure 3

Prelli Bozzo, Nchioua *et al.*

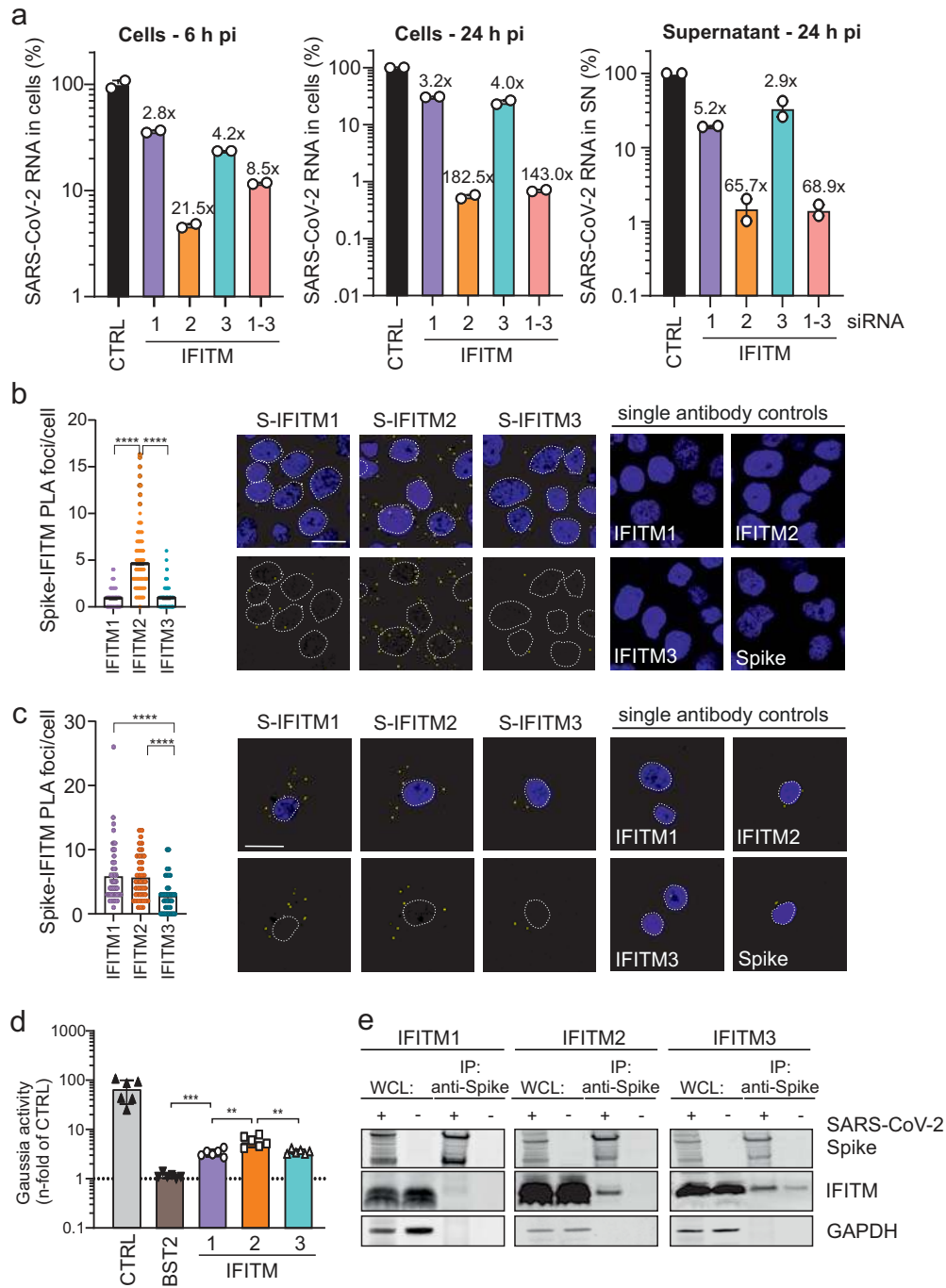


# Figure 4

Prelli Bozzo, Nchioua *et al.*

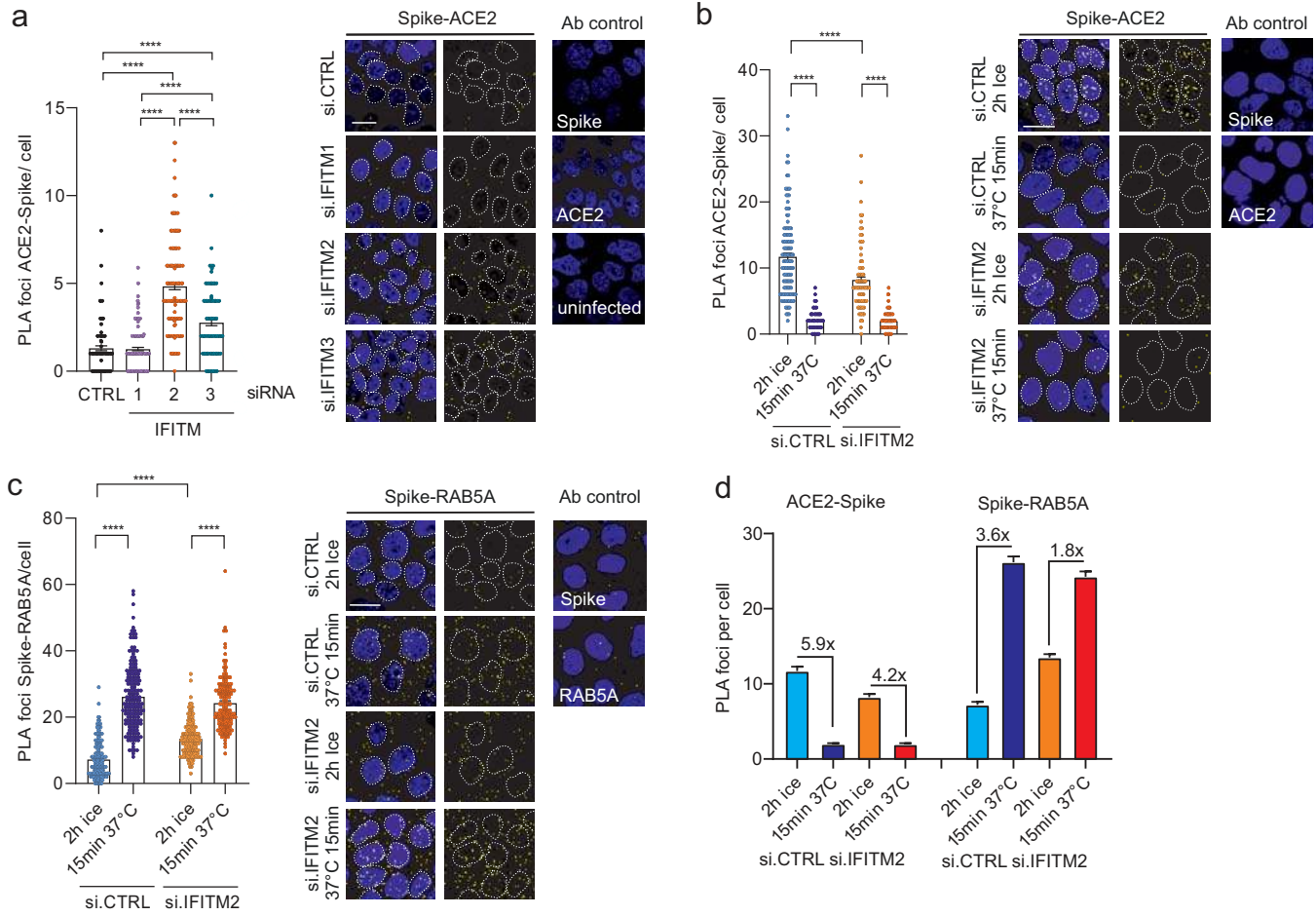


**Figure 5**

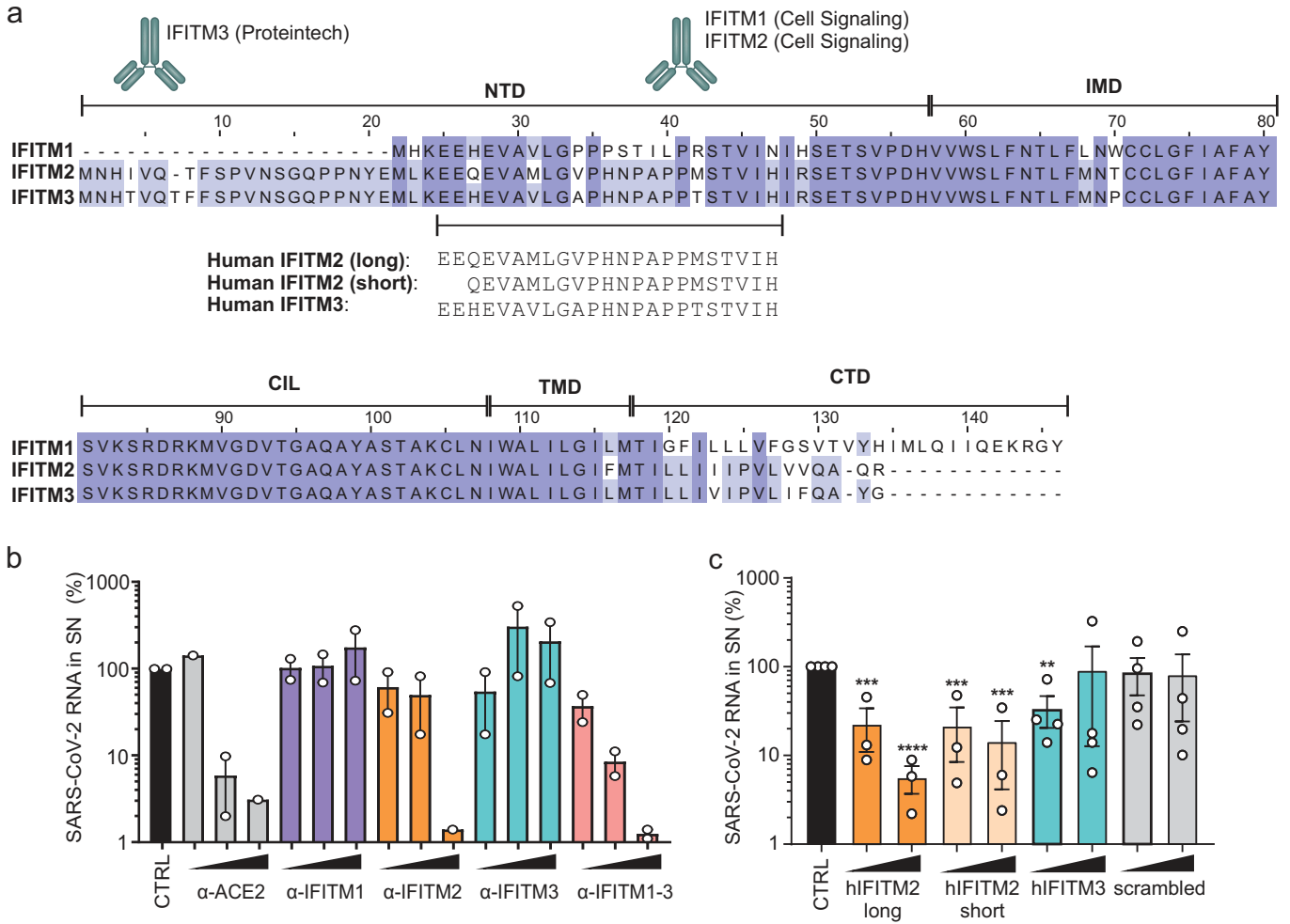


# Figure 6

Pirelli Bozzo, Nchioua *et al.*

